Biochemistry

Article

pubs.acs.org/biochemistry

Aberrantly Large Single-Channel Conductance of Polyhistidine Arm-Containing Protein Nanopores

Avinash Kumar Thakur,[†,‡] Motahareh Ghahari Larimi,[†] Kristin Gooden,[§] and Liviu Movileanu*[,†,‡,∥]

[†]Department of Physics, Syracuse University, 201 Physics Building, Syracuse, New York 13244-1130, United States

[‡]Structural Biology, Biochemistry, and Biophysics Program, Syracuse University, 111 College Place, Syracuse, New York 13244-4100, United States

[§]Department of Physics and Astronomy, University of Missouri, 223 Physics Building, Columbia, Missouri 65211-7010, United States

[∥]Department of Biomedical and Chemical Engineering, Syracuse University, 329 Link Hall, Syracuse, New York 13244, United States

Supporting Information

ABSTRACT: There have been only a few studies reporting on the impact of polyhistidine affinity tags on the structure, function, and dynamics of proteins. Because of the relatively short size of the tags, they are often thought to have little or no effect on the conformation or activity of a protein. Here, using membrane protein design and single-molecule electrophysiology, we determined that the presence of a hexahistidine arm at the N-terminus of a truncated FhuA-based protein nanopore, leaving the C-terminus untagged, produces an unusual increase in the unitary conductance to ~8 nS in 1 M KCl. To the best of our knowledge, this is the largest single-channel conductance ever recorded with a monomeric β-barrel outer membrane protein. The hexahistidine arm was captured by an anti-polyhistidine tag monoclonal antibody added to the side of the channel-forming protein addition, but not to the opposite side, documenting that this truncated FhuA-based protein nanopore inserts into a planar lipid bilayer with a preferred orientation. This finding is in agreement with the protein insertion *in vivo*, in which the large loops face the extracellular side of the membrane. The aberrantly large single-channel conductance, likely induced by a greater cross-sectional area of the pore lumen, along with the vectorial insertion into a lipid membrane, will have profound implications for further developments of engineered protein nanopores.

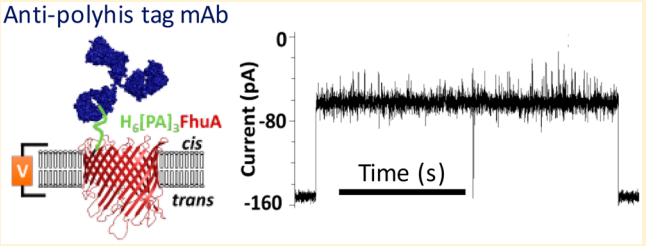

There is a pressing demand for the design and creation of novel protein nanopores in medical bionanotechnology.[1] The β-barrel remains one attractive protein scaffold,[2,3] because of the remarkable tractability to major modifications in its biophysical, biochemical, and structural features. The fundamental basis of this tractability and versatility of the β-barrel proteins is their unusually high thermodynamic stability. These traits are determined by the rich network of stabilizing hydrogen bonds among the antiparallel β-strands. Monomeric β-barrels are advantageous for protein redesign, because multimeric proteins require further purification steps for separating the targeted modified oligomer from other products of the oligomerization reaction.[4,5] Therefore, several groups pursued the engineering of these proteins for their use as a single-chain, pore-forming polypeptide for the precise alteration of their structure, chemical function, and folding dynamics at single-molecule resolution. For example, outer membrane protein G (OmpG) of *Escherichia coli* has received an increasing level of interest in the examinations of gating fluctuations[6,7] and development of stochastic sensing elements.[4,8,9] Moreover, studies of structure−function relationships were extended to other monomeric β-barrel proteins, such as outer membrane protein A (OmpA) of *E. coli*,[10] outer membrane carboxylate channels (Occ) of *Pseudomonas aeruginosa*,[11−14] ferric hydroxamate uptake component A (FhuA) of *E. coli*,[5,15−17] and mitochondrial voltage-dependent anion channel (VDAC).[18,19]

In this work, we demonstrate the unusual enhancement of the single-channel conductance of a monomeric β-barrel pore by fusing a hexahistidine arm to the N-terminus of the polypeptide chain. This β-barrel is a redesigned variant of ferric hydroxamate uptake A (FhuA) of *E. coli*, a 714-residue protein composed of 22 antiparallel β-strands.[20] These β-strands are connected to each other by 10 short β-turns (T) on the periplasmic side and 11 large extracellular loops (L) on the extracellular side. The X-ray crystal structure of the native FhuA protein[20] reveals a pore length of ~6.5 nm from the periplasmic to extracellular side, whereas the cross-sectional diameter varies at different locations of the pore lumen, it being 2.6 nm × 3.9 nm on the periplasmic opening and 2.6 nm × 3.6 nm on the extracellular entrance. These dimensions included the average length of the side chains of the internal residues. FhuA is a TonB-dependent transporter[21−23] that mediates the navigation of Fe^{3+} complexed by the siderophore ferrichrome across the outer membrane (OM) of Gram-negative bacteria.[15,17] In this

Received: June 19, 2017
Revised: August 15, 2017
Published: August 16, 2017

DOI: 10.1021/acs.biochem.7b00577
Biochemistry 2017, 56, 4895−4905

way, the lumen of the FhuA protein serves as a permeation conduit for the high-affinity, energy-driven uptake of Fe^{3+} into the bacterial cell, which is facilitated by the TonB complex to unplug the channel.[24] However, its primary role of Fe^{3+} transporter further extends to a number of antibiotics, including albomycin[25] and rifamycin.[26] Moreover, FhuA functions as a receptor for a number of bacteriophages, such as T1, T5, and ϕ80,[27−29] antimicrobial microcin J25 peptide,[30] and colicin M toxin.[31,32]

Only a few studies demonstrated the potential implications of polyhistidine affinity tags on the structure−function relationship of proteins. Prior explorations emphasized the alterations in structure,[33] stability,[34] and dynamics[35] of proteins depending on the location of the polyhistidine arm, fused to the C- or N-terminus of the recombinant protein. Some reports shared legitimate concerns that polyhistidine arms affect the enzymatic activity of proteins.[36−38] To the best of our knowledge, this is the first single-molecule examination of the major changes in the electrical signature of a transmembrane protein pore by a fused polyhistidine arm. An extensive truncation FhuA mutant, featuring the deletion of an N-terminal, 160-residue cork domain and most of the five large extracellular loops, L3−L5, L10, and L11, simply named tagless FhuA (TL-FhuA), showed a single-channel conductance of ∼4 nS in 1 M KCl (Figure 1).[39] In this way, FhuA was converted

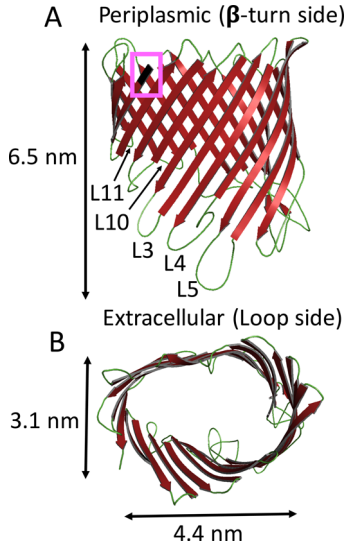

Figure 1. Ribbon diagram of tagless truncated FhuA (TL-FhuA) protein derived through homology modeling: (A) side view of TL-FhuA and (B) top view of TL-FhuA, which was taken from the periplasmic side. The luminal dimensions of TL-FhuA, as determined from C_α to C_α, were inferred from the X-ray crystal structure of the native FhuA (FhuA). The N-terminus of the pore is colored black.

from a non-ion-conducting OM protein to an ion-conducting β-barrel nanopore, whose large unitary conductance was greater than those values previously recorded under different contexts.[15] These situations included other truncation FhuA mutants[40,41] as well as single-channel conductance values measured by the interactions of FhuA with bacteriophage T5.[42]

Here, we show that the fusion of a hexahistidine arm to the N-terminus of the TL-FhuA protein, leaving the C-terminus untagged, produced a unitary conductance of ∼8 nS. This aberrant conductance likely resulted from a drastic change in the overall shape of the pore lumen. Interactions of a short and positively charged peptide with the FhuA pore lumen confirmed its monomeric nature. Moreover, we were able to probe transient captures of the hexahistidine arm when an anti-hexahistidine tag monoclonal antibody (mAb) was added to the side of the channel-forming protein addition, but not to the opposite side. This finding suggests that the hexahistidine arm was indeed accessible to the aqueous phase. In addition, this aberrant conductance of ∼8 nS was also noted when the hexahistidine arm was fused to the C-terminus of the TL-FhuA protein, which is within ∼0.7 nm of the N-terminus.

EXPERIMENTAL METHODS

Design and Mutagenesis of the Expression Constructs. All the designed genes were constructed using conventional polymerase chain reaction (PCR) and cloned into expression vector pPR-IBA1 using the BsaI restriction site. The *tl-fhua* gene was amplified from the *fhua* Δ*c*/Δ5*l* plasmid[39] using the forward primer 5′-CGG CGG TCT CCA ATG CTG AAA GAA GTT CAG TT-3′ and the reverse primer 5′-GGA GGT CTC CGC GCT TTA AAA ACG AAAG-3′. *fhua* Δ*c*/Δ5*l* lacked the regions encoding the cork domain (C) and extracellular loops L3−L5, L10, and L11, as compared to wild-type *fhua*. TL-FhuA has no tags at the N- or C-terminus. The $[pa]_3$*fhua* gene, which encodes three repeats of PA at the N-terminus of TL-FhuA, was constructed using the forward primer 5′-TAT ACG GTC TCC AAT GCC TGC TCC CGC CCC AGC ACT GAA AGAA-3′, the reverse primer 5′-GGA GGT CTC CGC GCT TTA AAA ACG AAAG-3′, and the *tl-fhua* plasmid as template DNA. The $h_6[pa]_3$*fhua* gene, which encodes the six-His tag and $[PA]_3$ at the N-terminus of TL-FhuA, was constructed using the forward primer 5′-TAT AGG TCT CGA ATG CAC CAT CAC CAT CAC CAT CCT GCT CCC GCC CCA-3′, the reverse primer 5′-GGA GGT CTC CGC GCT TTA AAA ACG AAA G-3′, and the $[pa]_3$*fhua* plasmid as template DNA. Similarly, the h_6*fhua* gene, which encodes the six-His tag at the N-terminus of TL-FhuA, was constructed using the forward primer 5′-TAT ACG GTC TCC AAT GCA CCA TCA CCA TCA CCA TCT GAA A-3′, the reverse primer 5′-GGA GG TCT CCG CGC TTT AAA AAC GAA AG-3′, and the $h_6[pa]_3$*fhua* plasmid as template DNA. The *fhua*$[ggs]_4h_6$ gene encoding the six-His tag and $[GGS]_4$ at the C-terminus of TL-FhuA was constructed using two rounds of PCR. First, the *fhua*$[ggs]_4$ gene was constructed using the forward primer 5′-TAT ACG GTC TCC AAT GCT GAA AGA AGT TC-3′, the reverse primer 5′-AAC ACT ACC ACC ACT ACC ACC GCT GCC GCC GCT GCC GCC AAA ACG AAA GGT TGC GG-3′, and the *tl-fhua* plasmid as template DNA. The second round of PCR was performed using the *fhua*$[ggs]_4$ gene as template DNA, along with the forward primer 5′-TAT ACG GTC TCC AAT GCT GAA AGA AGT TC-3′ and the reverse primer 5′-GAA GAG CGC CGA GAC CTT AAT GGT GAT GGT GAT GGT GAC TAC CAC CAC T-3′.

Protein Expression and Purification. All the *fhua* gene variants were transformed into *E. coli* BL21 (DE3) cells. The ampicillin-resistant transformed cells were grown in 1 L of Luria-Bertani (LB) medium at 37 °C until OD_{600} reached ∼0.5, at which time the protein expression was induced by 0.5 mM isopropyl β-D-1-thiogalactopyranoside (IPTG). Cells were further grown for an additional 3−4 h until the cell growth plateaued, as measured by OD_{600}. Then, cells were harvested by centrifugation at 3700*g* for 30 min at 4 °C. Cell lysis was accomplished using a model 110L microfluidizer (Microfluidics,

DOI: 10.1021/acs.biochem.7b00577
Biochemistry 2017, 56, 4895−4905

Newton, MA). Cell lysates were centrifuged at 3700*g* for 20 min at 4 °C to separate the insoluble pellets from the supernatant. Next, the pellets were washed by being resuspended in 300 mM KCl, 50 mM Tris-HCl, and 5 mM EDTA (pH 8) and spun down at 11200*g* for 20 min at 4 °C. This process was repeated, followed by two washes with 300 mM KCl, 50 mM Tris-HCl, 5 mM EDTA, and 0.5% Triton (pH 8) and a final wash with 50 mM Tris-HCl (pH 8). To purify TL-FhuA and $[PA]_3$FhuA, washed pellets were solubilized in the denaturing buffer, containing 50 mM Tris-HCl (pH 8) and 8 M urea, and loaded onto an anion exchange column (Bio-Rad, Hercules, CA), which was equilibrated with the same denaturing buffer. Proteins were eluted using a linear gradient of 1000 mM KCl, 50 mM Tris-HCl (pH 8), and 8 M urea. Washed $H_6[PA]_3$FhuA and H_6FhuA pellets were solubilized in the denaturing buffer containing 500 mM KCl, 50 mM Tris-HCl (pH 8), and 8 M urea. The protein-containing solutions were filtered using 0.2 μm filters (Thermo Fisher Scientific, Rochester, NY) and loaded onto a 5 mL Ni-NTA column (Bio-Rad), which was equilibrated with the same denaturing buffer, via a BioLogic DuoFlow chromatography system (Bio-Rad). Then, the column was washed with 500 mM KCl, 50 mM Tris-HCl (pH 8), 8 M urea, and 6 mM imidazole. The proteins were eluted with 500 mM KCl, 50 mM Tris-HCl (pH 8), 8 M urea, and 300 mM imidazole. All the fractions were analyzed using sodium dodecyl sulfate−polyacrylamide gel electrophoresis for purity levels of >95%. Pure fractions were pulled out and dialyzed extensively against doubly distilled H_2O. Dialyzed fractions were lyophilized and stored at −80 °C.

Protein Refolding. Lyophilized protein samples were solubilized in 200 mM KCl, 8 M urea, and 50 mM Tris-HCl (pH 8) for 2 h at a final concentration of 30−50 μM. Then, all denatured proteins were refolded through rapid dilution.[43] In addition, TL-FhuA was also refolded through a dialysis protocol.[39] In the case of rapid dilution, denatured protein samples were quickly diluted into the cold refolding buffer, containing 200 mM KCl, 0.5% *n*-dodecyl β-D-maltopyranoside (DDM), and 20 mM Tris-HCl (pH 8.0), and incubated for >48 h at 4 °C. To refold TL-FhuA via dialysis, the denatured protein samples were incubated in 1.5% DDM. They were dialyzed against the refolding buffer containing 200 mM KCl and 20 mM Tris-HCl (pH 8) at 4 °C for >48 h at 4 °C. Then, the refolded protein sample was passed through a Superdex 200 HR size-exclusion chromatography column, which was equilibrated with 200 mM KCl, 20 mM Tris-HCl (pH 8), and 0.5% DDM, using a BioLogic DuoFlow chromatography system (Bio-Rad). Protein concentrations were determined by their molar absorptivity at a wavelength of 280 nm.

Single-Channel Electrical Recordings. All single-channel electrical recordings were conducted at room temperature using planar lipid bilayers with 1,2-diphytanoyl-*sn*-glycero-phosphocholine (Avanti Polar Lipids, Alabaster, AL), as previously described.[44,45] The lipid bilayers were formed across a 100 μm diameter aperture in a 25 μm thick Teflon film (Goodfellow Corp., Malvern, PA), which separated the *cis* and *trans* compartments. The aperture was pretreated with hexadecane (Sigma-Aldrich, St. Louis, MO) dissolved in highly purified pentane (high-performance liquid chromatography grade, Fisher, Fair Lawn, NJ) at a concentration of 10% (v/v). The refolded proteins were added to the *cis* compartment at a final concentration of 0.3−1.3 ng/μL. The *cis* compartment was grounded. The single-channel currents were recorded using an Axopatch 200B patch-clamp amplifier (Axon Instruments, Foster City, CA). The electrolyte solution contained 1000 mM KCl and 10 mM Tris-HCl (pH 8). The single-channel currents were low-pass filtered with an eight-pole Bessel filter (model 900, Frequency Devices, Ottawa, IL) at a frequency of 10 kHz and sampled at 50 kHz, unless otherwise stated. A desktop personal computer was equipped with a DigiData 1440A A/D converter (Axon) for the acquisition of data. For both acquisition and analysis of data, we used the pClamp 10.5 software package (Axon). In the case of the mouse mAb binding experiment, the *cis* compartment buffer was washed out with the fresh buffer before the addition of mAb to the chamber. The anti-hexahistidine tag mAb was purchased from Genscript (Piscataway, NJ).

RESULTS

Discovering an Unusual High-Conductance Open State of a Monomeric β-Barrel. Recent single-channel recordings demonstrated that a truncation FhuA mutant lacking the 160-residue cork domain and five extracellular loops (L3−L5, L10, and L11) exhibits an open-state conductance of ∼4 nS.[39] Indeed, we confirmed that the unitary conductance histogram of TL-FhuA, a truncation FhuA derivative with no tags, showed two major peaks, a low-conductance peak centered at ∼2.5 ± 0.1 nS (N = 41 distinct single-channel insertions) and an open-state conductance peak centered at ∼4.0 ± 0.1 nS (N = 43) (Figure 2A and Figure S1A). For the sake of clarity in this section, we denote the numbers of distinct single-channel insertions and independent single-channel experiments with N and n, respectively. Surprisingly, we

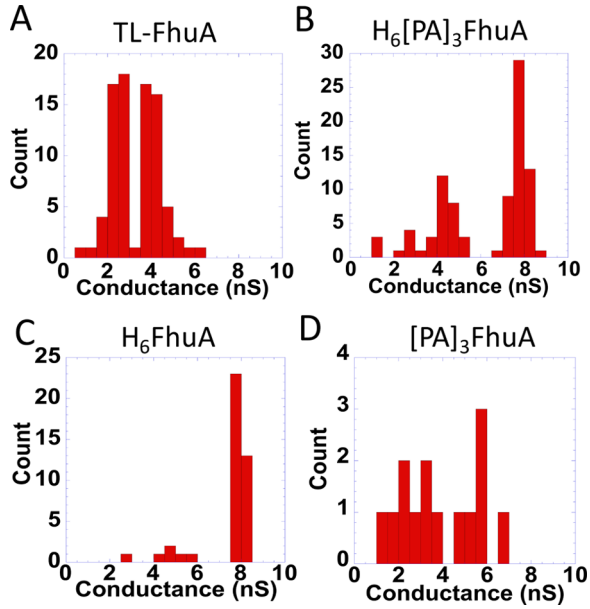

Figure 2. Single-channel conductance histogram of four truncation FhuA variants: (A) TL-FhuA, a truncation FhuA derivative with no tags; (B) $H_6[PA]_3$FhuA, a truncation FhuA mutant containing a six-His tag and a $[PA]_3$ linker at the N-terminus; (C) H_6FhuA, a truncation FhuA variant containing a six-His tag at the N-terminus; and (D) $[PA]_3$FhuA, a truncation FhuA variant containing a $[PA]_3$ linker at the N-terminus. The measurements were performed using an electrolyte solution containing 1 M KCl and 10 mM Tris-HCl (pH 8.0). The single-channel conductance histograms were derived using data points resulting from several multichannel insertion experiments. The single-channel conductance values were determined at a transmembrane potential of 20 mV.

DOI: 10.1021/acs.biochem.7b00577
Biochemistry 2017, 56, 4895−4905

noted that the single-channel insertion of $H_6[PA]_3$FhuA, a truncation FhuA mutant containing a six-His tag and a $[PA]_3$ linker at the N-terminus, into a planar lipid bilayer displayed a substantial increase in open-state conductance, from ~4 nS for TL-FhuA to 7.8 ± 0.1 nS (N = 53) (Figure 2B and Figure S1B). In addition, this engineered protein nanopore exhibited another low-conductance peak centered at 4.4 ± 0.1 nS (N = 32). Notably, the single-channel electrical signatures of the ~4 nS substates of TL-FhuA and $H_6[PA]_3$FhuA were distinctive from each other (Figure S2), in which TL-FhuA was quieter than $H_6[PA]_3$FhuA. At a transmembrane potential of ≤20 mV, $H_6[PA]_3$FhuA exhibited more frequent current blockades at negative potentials (Figure S3A,B). However, at voltages of at least ±40 mV, this nanopore showed long-lived current blockades with a normalized current blockade, I/I_0, of 49 ± 14% (n = 4), where I and I_0 indicate the average current blockade and amplitude of the unitary current, respectively (Figure S3C).

On the basis of these findings, we judged that the observed significant increase in the unitary conductance of $H_6[PA]_3$FhuA with respect to TL-FhuA could be due to the presence of $[PA]_3$, H_6, or both. To investigate this further, we developed two truncation FhuA variants: H_6FhuA, featuring the fusion of H_6 to the N-terminus of TL-FhuA, and $[PA]_3$FhuA, featuring the fusion of $[PA]_3$ to the N-terminus of TL-FhuA. Indeed, the H_6FhuA single-channel conductance histogram displayed a peak centered at 8.0 ± 0.1 nS (N = 36) (Figure 2C and Figure S1C). As a distinctive property of H_6FhuA with respect to $H_6[PA]_3$FhuA, these protein nanopores often showed long-lived current blockades [I/I_0 = 43 ± 11% (n = 4)] at applied transmembrane potentials of at least ±20 mV (Figure S3D). On the other hand, $[PA]_3$FhuA failed to show a uniform single-channel conductance, despite numerous attempts. Specifically, the single-channel conductance histogram showed a broad distribution, in the range of 1.5−7.0 nS (n = 12) (Figure 2D). The protein nanopore with the most reproducible electrical signature had a conductance of ~5.5 nS (n = 3). Moreover, in contrast to TL-FhuA, which showed no single-channel current blockades at 20 mV, the most reproducible electrical signature of $[PA]_3$FhuA displayed a noisy electrical signature with transient current blockades having I/I_0 values between 30 and 85% (Figure S4. Therefore, we conclude that H_6 is critical for forming a high-conductance open-state conformation of the truncated FhuA protein within a lipid bilayer.

Far-ultraviolet circular dichroism (CD) experiments were conducted to ensure proper folding of all truncation FhuA mutants under detergent solvation conditions. Indeed, the CD spectra of all truncation FhuA variants looked quite similar to each other, displaying minima at a wavelength of ~218 nm, which is indicative of a folded β-sheet structure (Figure S5).[46,47] Because θ is dependent on the reciprocal of protein concentration and the number of peptide bonds, distinctions in these numbers among all truncation FhuA derivatives produced small alterations in the molar ellipticity from one mutant to another.

Moreover, we also performed urea-induced protein unfolding experiments to determine whether these truncation FhuA variants show any distinction in terms of their thermodynamic stability, which could be related to their differences in pore forming activity. The chemical denaturant-induced unfolding data were obtained by exciting the protein at a wavelength of 280 nm and monitoring the tryptophan fluorescence in the range of 310−420 nm (Figure S6 and Table S1).[10] The unfolding of individual FhuA derivatives was monitored by the change in the wavelength of maximum emission (λ_{max}). The equilibrium unfolding curves for all the FhuA variants followed a two-state model. The fit of the unfolding curves with a symmetrical sigmoidal function permitted the determination of urea concentration at the midpoint of the unfolding transition, C_m, and the cooperativity parameter, m. The thermodynamic stability of the truncation FhuA derivatives in proteomicelles was expressed in terms of the free energy of unfolding, ΔG°_u, where $\Delta G^\circ_u = mC_m$. Notably, all truncation FhuA derivatives exhibited closely similar thermodynamic stability parameters in the aqueous phase with a midpoint of the unfolding transition, C_m, located at ~4 M and an unfolding free energy, ΔG°_u, of ~2.6 kcal/mol.

$H_6[PA]_3$FhuA Is a Monomeric Protein Nanopore. Here, we were interested in examining whether $H_6[PA]_3$FhuA is a dimer, because it shows a double conductance of that exhibited by TL-FhuA, or is a new high-conductance open substate. TL-FhuA always inserted into a lipid bilayer in a single orientation, as judged by its asymmetric values of the current amplitudes at positive and negative biases. For example, at a transmembrane potential of 40 mV, the unitary current difference of TL-FhuA $\Delta I = I_+ - I_- = -5 \pm 1$ pA (n = 8), where I_+ and I_- are the current amplitudes at positive and negative transmembrane potentials, respectively. The unitary current values at positive and negative biases were ~162 and −167 pA, respectively (n = 8). If $H_6[PA]_3$FhuA was a dimer, then this current asymmetry of the negative voltage with respect to positive voltage would have increased. Instead, the $H_6[PA]_3$FhuA protein nanopore showed an opposite current asymmetry with respect to that of TL-FhuA at the same transmembrane potential [$\Delta I = 4 \pm 1$ pA (n = 8)]. The unitary current values at positive and negative biases were ~318 and ~−314 pA, respectively (n = 8). We further explored the interaction of Syn B2,[48−50] a short positively charged polypeptide, with both TL-FhuA and $H_6[PA]_3$FhuA. Syn B2 is a 23-residue polypeptide with five positive charges and, therefore, is prone to interact with the acidic lumen of FhuA.[20] When inserted into a planar lipid bilayer, TL-FhuA showed no events at an applied transmembrane potential of 20 mV (Figure S3A). In contrast, $H_6[PA]_3$FhuA displayed transient current blockades at a rate of 1.5 ± 0.7 s^{-1} (n = 3) with I/I_0 being between 10 and 65% (Figure 3A).

In the presence of 10 μM Syn B2 added to the *trans* side, TL-FhuA displayed infrequent current blockades at a frequency of 0.32 ± 0.08 s^{-1} (n = 3) with I/I_0 being between 10 and 35% (Figure 3B). In contrast, when $H_6[PA]_3$FhuA was employed, 10 μM Syn B2 added to the *trans* side produced very frequent current blockades at a rate of 186 ± 35 s^{-1} (n = 3) with I/I_0 being between 10 and 100% (Figure 3C). This finding indicates that there was a drastic alteration in the nature of the attractive electrostatic interactions between positively charged Syn B2 and the dense negative charge distribution within the FhuA pore lumen.[20] If $H_6[PA]_3$FhuA were a dimer, then the frequency of current blockades would have been double that frequency of individual monomers. Instead, we discovered a 580-fold increase in the event frequency. Moreover, the amplitude of these Syn B2-produced current blockades was in a range of >50% of the unitary current, which is in accord with a monomeric structure of $H_6[PA]_3$FhuA in a lipid bilayer. Otherwise, Syn B2 would have produced current blockades in two steps for a dimer.

DOI: 10.1021/acs.biochem.7b00577
Biochemistry 2017, 56, 4895−4905

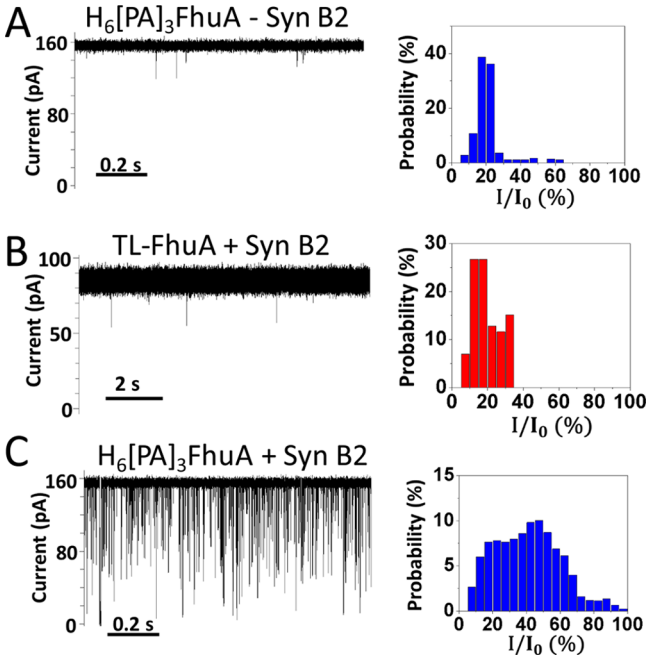

Figure 3. Experimental evidence of the monomeric nature of $H_6[PA]_3$FhuA. (A) Representative single-channel electrical recording of $H_6[PA]_3$FhuA without Syn B2 (left), along with its corresponding normalized event−amplitude histogram, I/I_0 (right). (B) Representative single-channel electrical recording of TL-FhuA in the presence of 10 μM Syn B2 added to the *trans* side (left), along with its corresponding normalized event−amplitude histogram, I/I_0 (right). (C) Representative single-channel electrical recording of $H_6[PA]_3$FhuA in the presence of 10 μM Syn B2 added to the *trans* side (left), along with its corresponding normalized event−amplitude histogram, I/I_0 (right). Other experimental conditions were the same as those described in the legend of Figure 2. The transmembrane potential was 20 mV. For the sake of clarity, all the electrical traces were low-pass Bessel filtered at a frequency of 7 kHz.

Is the Hexahistidine Arm Tightly Bound to the β-Barrel Scaffold of $H_6[PA]_3$FhuA? Here, we asked if the hexahistidine arm strongly interacted with the FhuA scaffold, thereby providing some mechanical stability for this high-unitary conductance, open-state conformation. Therefore, we examined the ability to capture the six-His tag outside the pore lumen via a transient binding with an anti-His tag monoclonal antibody (mAb). This experiment also targeted the question of whether the six-His tag was accessible to the aqueous phase on either the periplasmic or cytoplasmic side of the protein. If the six-His tag were exposed at least in part, it would have been sampled by the presence of mAb in solution. In the absence of mAb, $H_6[PA]_3$FhuA displayed events with the following three distinct dwell times: $\tau_1 = 0.02 \pm 0.01$ ms ($p = 0.45 \pm 0.17$; I/I_0 ranging from 10 to 30%), $\tau_2 = 1.0 \pm 0.4$ ms ($p = 0.47 \pm 0.22$; I/I_0 ranging from 30 to 50%), and $\tau_3 = 21 \pm 8$ ms ($p = 0.09 \pm 0.05$; I/I_0 ranging from 30 to 50%) (for all values, $n = 4$) (Figure 4). The very short dwell time, τ_1, was extrapolated from the fitting curve and assuming the contribution of missing events because of limited time resolution.[51,52] The addition of 67 nM mAb to the *cis* compartment (e.g., the side of the channel-forming protein addition) resulted in reversible and very long-lived current blockades (Figure 5 and Figure S7). The very long-lived current blockades were on the order of one minute to several minutes, with a normalized current (I/I_0) of 83.78 ± 8.54% ($n = 3$), indicative of a strong binding interaction of the mAb−six-His tag complex.[53] It is worth mentioning that these long-lived events were never noted in the absence of mAb.

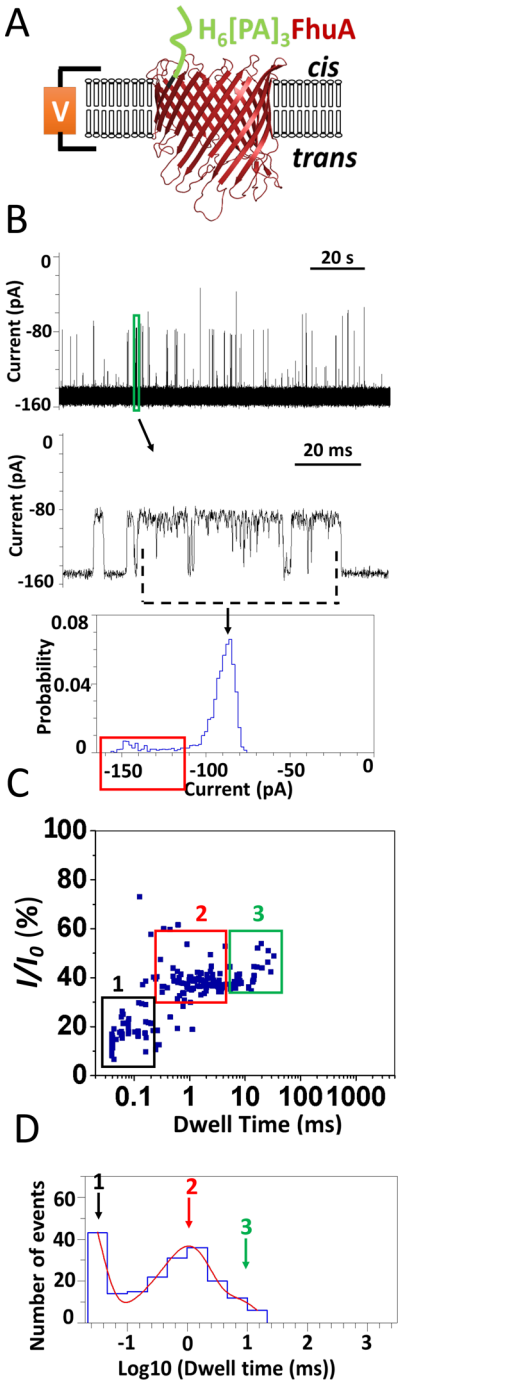

Figure 4. Single-channel electrical signature of $H_6[PA]_3$FhuA. (A) Schematic model of $H_6[PA]_3$FhuA. (B) Representative single-channel electrical recording of $H_6[PA]_3$FhuA. One representative event is highlighted in green, along with an expanded trace and its normalized all-point current amplitude histogram. (C) Semilog scatter plot of I/I_0 vs dwell time of the events of $H_6[PA]_3$FhuA. (D) Dwell time histogram in a semilogarithmic representation. The transmembrane potential was −20 mV. Other experimental conditions were the same as those described in the legend of Figure 2. For the sake of clarity, all the electrical traces were low-pass Bessel filtered at a frequency of 7 kHz.

DOI: 10.1021/acs.biochem.7b00577
Biochemistry 2017, 56, 4895−4905

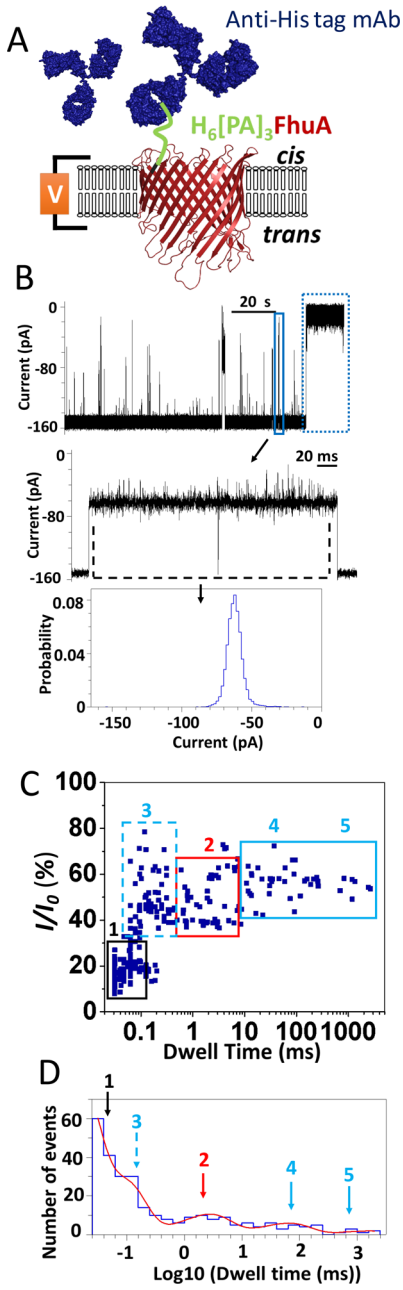

Figure 5. Transient captures of the mouse monoclonal anti-six-His tag antibody (mAb) using $H_6[PA]_3$FhuA. (A) Schematic model of $H_6[PA]_3$FhuA in the presence of mAb. (B) Representative single-channel electrical recording of $H_6[PA]_3$FhuA in the presence of 67 nM mAb added to the *cis* side of the membrane. The representative reversible mAb−six-His binding event is colored dark blue, along with an expanded trace and its normalized all-point current amplitude histogram, whereas the very long-lived mAb−six-His binding event is shown with a dotted blue line. (C) Semilog scatter plot of I/I_0 vs dwell time of the events of $H_6[PA]_3$FhuA in the presence of mAb added to the *cis* side. (D) Dwell time histogram in a semilogarithmic representation. The transmembrane potential was −20 mV. Other experimental conditions were the same as those in Figure 2. For the sake of clarity, all the electrical traces were low-pass Bessel filtered at a frequency of 7 kHz.

Reversible current blockades resulted in five distinct dwell times, two of which were closely similar to the $H_6[PA]_3$FhuA nanopore's events, namely, $\tau_1' = 0.02 \pm 0.01$ ms ($p = 0.67 \pm 0.07$; I/I_0 ranging from 10 to 30%) and $\tau_2' = 2.7 \pm 0.1$ ms ($p = 0.11 \pm 0.02$; I/I_0 ranging from 40 to 60%), whereas the other three event types were likely due to the mAb−six-His tag interaction. Their mean durations were as follows: $\tau_3' = 0.15 \pm 0.12$ ms ($p = 0.15 \pm 0.09$; I/I_0 ranging from 40 to 80%), $\tau_4' = 61 \pm 11$ ms ($p = 0.05 \pm 0.01$; I/I_0 ranging from 50 to 60%), and $\tau_5' = 1800 \pm 690$ ms ($p = 0.02 \pm 0.01$; I/I_0 ranging from 50 to 60%) (for all values, $n = 3$). Because the τ_3' dwell time was very short, this event likely resulted from the frequent collisions of mAb with the pore opening, but without a specific mAb−six-His tag binding interaction. The τ_4' population appears to be close to the τ_3 value, although these two events are different in their electrical signature (Figures 4B and 5B). For instance, the τ_3 event was decorated by short-lived recovery current transitions to the fully open state, whereas τ_4' did not exhibit this feature, which was indicative of a continuous mAb−six-His tag binding event. Because the anti-His tag mAb can also sample binding interactions with the four-His and five-His stretches of the hexahistidine arm,[54,55] this property explains, at least in part, why we noted multiple binding dwell times. In other words, the very long-lived current blockade likely occurred because of the binding of the hexahistidine arm, whereas τ_4' and τ_5' were potentially determined by the binding of four-His and five-His stretches of the hexahistidine arm, respectively.

The binding of mAb to the six-His tag in the *cis* compartment points out the specific orientation of $H_6[PA]_3$FhuA in the planar lipid bilayer. $H_6[PA]_3$FhuA inserts into the bilayer in a single orientation via extracellular loops first. This hypothesis was also confirmed with a control experiment in which $H_6[PA]_3$FhuA was examined in the presence of 67 nM mAb added to the *trans* side. Indeed, no significant change in the electrical signature, which pertained to the specific mAb−six-His tag binding, was observed (Figure 6). The three observed types of events were closely similar to the current blockades of $H_6[PA]_3$FhuA in the absence of mAb, with the following average dwell times: $\tau_1^* = 0.02$ ms ($p = 0.67$; I/I_0 ranging from 10 to 30%), $\tau_2^* = 1.1$ ms ($p = 0.23$; I/I_0 ranging from 25 to 50%), and $\tau_3^* = 8.5$ ms ($p = 0.1$; I/I_0 ranging from 35 to 50%). The absence of the short-lived collision events noticed when the mAb was added to the *cis* side can be explained by the long protrusion of the β-barrel into the aqueous phase, so these events were electrically silent in this case. The outcomes of these experiments suggest that the hexahistidine arm was exposed to only the *cis* side and not permanently bound to the β-barrel scaffold of $H_6[PA]_3$FhuA.

Is the N-Terminus Essential for Attaining the Unusually High Single-Channel Conductance of Hexahistidine Arm-Containing FhuA? Given that the ~8 nS conductance open state was noted using the two independent hexahistidine arm-containing truncation FhuA mutants, we asked whether this outcome was dependent on the choice of the N-terminus. The homology structure of the truncation TL-FhuA mutant (Figure 1) indicates a relatively short distance of ~0.7 nm between the C- and N-termini. Therefore, a fusion site at the C-terminus would introduce the hexahistidine arm almost at the same location of the pore lumen near its periplasmic opening. Interestingly, the reconstitution of the FhuA$(GGS)_4H_6$ protein into a planar lipid membrane again revealed a high-conductance open state with a unitary value of 7.7 ± 0.2 nS ($n = 5$) (Figure S8), indicating that this unusual outcome was independent of the type of terminus. Moreover, the use of a $(GGS)_4$ polypeptide substantially longer and more flexible than $(PA)_3$ confirmed that the linker between the

DOI: 10.1021/acs.biochem.7b00577
Biochemistry 2017, 56, 4895−4905

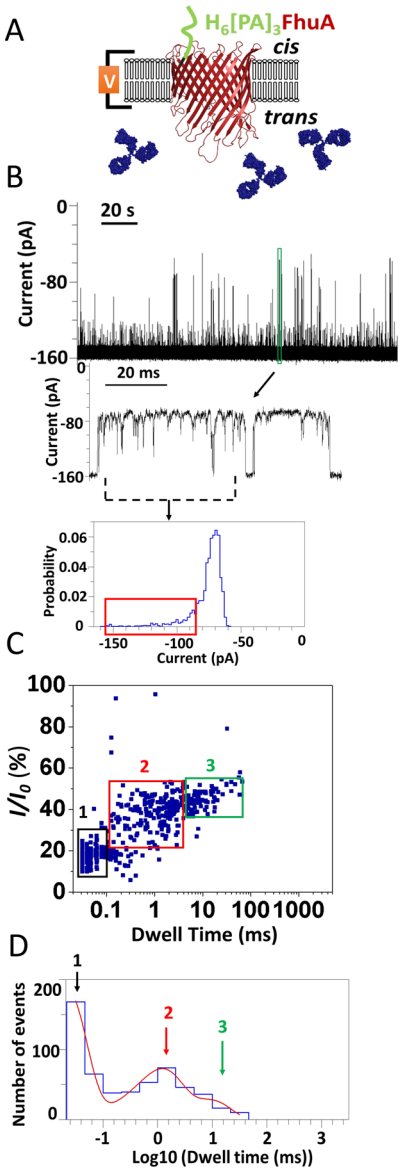

Figure 6. Single-channel electrical signature of $H_6[PA]_3$FhuA when mAb was added to the *trans* side. (A) Schematic model of $H_6[PA]_3$FhuA in the presence of mAb added to the *trans* side. (B) Single-channel electrical recording of $H_6[PA]_3$FhuA in the presence of 67 nM mAb added to the *trans* side of the membrane. The representative event of $H_6[PA]_3$FhuA is colored green, along with an expanded trace and its normalized all-point current amplitude histogram. (C) Semilog scatter plot of I/I_0 vs dwell time of the events of $H_6[PA]_3$FhuA in the presence of 67 nM mAb added to the *trans* side. (D) Dwell time histogram in a semilogarithmic representation. The transmembrane potential was −20 mV. Other experimental conditions were the same as those described in the legend of Figure 2. For the sake of clarity, all the electrical traces were low-pass Bessel filtered at a frequency of 7 kHz.

hexahistidine arm and terminus does not preclude the attainment of this high-conductance open state of the truncation FhuA mutant. The high-conductance open states of ∼8 nS, regardless of the choice of the terminus for the hexahistidine arm fusion, can be explained at least in part by the proximal location of the N- and C-termini.

DISCUSSION

In this work, we provide compelling experimental evidence of the existence of the aberrant, high-conductance open state of a hexahistidine arm-containing FhuA protein lacking the N-terminal cork domain and multiple extracellular loops. To the best of our knowledge, this is the highest single-channel conductance ever observed with a monomeric β-barrel OM protein. Such an unusually high single-channel conductance was noted with three independently prepared truncation FhuA derivatives, which differed from each other by both the terminus at which the hexahistidine arm was fused and the nature of the linker, a stiff $(PA)_3$ versus a highly flexible $(GGS)_4$ polypeptide. We noted a substantial increase in the channel conductance to values near ∼8 nS, indicating that the hexahistidine arm-containing truncation FhuA mutants likely exhibited a change in the cross-sectional area of the pore lumen.

The X-ray crystal structure of the homologous truncated FhuA protein reveals a variable internal diameter between 2.6 and 3.9 nm.[20] If the β-barrel of FhuA would maintain its lumen dimensions in the absence of the cork domain, with an average internal radius of ∼3.3 nm, and we assume that the voltage drop occurs across the entire length of the pore of ∼6.5 nm, then we obtain a unitary conductance of ∼9.9 nS in 1 M KCl. This value was inferred by assuming the contribution of the access resistance to the total resistance of the pore.[56,57] Such a unitary conductance is even greater than the high conductance of the new open state, as obtained by the fusion of the hexahistidine arm to one of the termini of the truncated TL-FhuA protein. Because the dimensions mentioned above were crystallographically determined using a native FhuA protein, it is likely that the internal cork domain of the protein has a stabilizing effect on the conformation and shape of the β-barrel scaffold.

Very recently, using cryo-electron microscopy and two-dimensional crystallization, we showed that the c-ring complex of the V_0 sector of V-ATPase forms a transmembrane protein pore with a cylindrical shape, whose internal diameter is ∼3.5 nm, whereas the pore length measures ∼6.5 nm.[45] Interestingly, this protein complex, reconstituted into a planar lipid membrane, exhibited channel forming ability with a unitary conductance of ∼8.3 nS. The Delcour group has extensively examined the wild type and various truncation mutants of the PapC usher of *E. coli*, a dimeric pore complex, whose individual monomers consist of a 24-stranded β-barrel channel, along with an occluding, 76-residue cork domain, as well as globular N- and C-terminal domains located on the periplasmic side.[58,59] The inner dimensions of the cross-sectional area of the 24-strand β-barrel protein pore are ∼2.5 nm × 4.5 nm. It was discovered that the removal of the plug domain of the PapC dimer, leaving a blocking α-helix domain, resulted in an increase in the single-channel conductance with two individual peaks of ∼3.0 and ∼7.3 nS for the monomer and dimer open states, respectively.[58]

Single-channel electrophysiology, along with solid-state nuclear magnetic resonance spectroscopy and molecular dynamics (MD) simulations, showed that the mitochondrial voltage-dependent anion channel (VDAC), a 19-strand monomeric β-barrel, undergoes cross-sectional shape fluctuations that were affected by the presence of an N-terminal α-helix.[18] The removal of this N-terminal α-helix led to an intermediate single-channel electrical signature affecting both the open and closed substates of VDAC. Interestingly,

DOI: 10.1021/acs.biochem.7b00577
Biochemistry 2017, 56, 4895−4905

computational electrophysiology determinations via MD simulations demonstrated that the deletion of the N-terminal α-helix of VDAC, while the overall structure remained unaltered, produced a substantial increase in single-channel conductance from ~4.2 to ~6.7 nS. The electrophysiology measurements revealed that such a truncation mutant exhibited a reduced unitary conductance at the closed-state levels of the wild-type VDAC protein and an increased current noise, indicating that the N-terminal α-helix has a rather stabilizing effect on the cross-sectional shape of the pore lumen.

The biophysical mechanism for driving this high-conductance substate of hexahistidine arm-containing FhuA remains unclear. We postulate that one of the two possibilities can explain this finding. First, the expanded β-barrel structure corresponding to the high-conductance open substate might be inherited from the very early stages of the refolding process, which was mediated by the solubilizing detergents. TL-FhuA might be prone to forming a semicollapsed structure with a ~4 nS conductance, which would be prevented, otherwise, by the presence of a polyhistidine cluster at the N- or C-terminus of TL-FhuA. Breathing conformational fluctuations of the monomeric β-barrel scaffold either in a reversible[6] or irreversible[18,60] fashion were reported previously. Second, at least one histidine residue might strongly interact with the cluster of negatively charged aspartic acids located on β-turn T1, which is in the proximity of the N- and C-termini (Figure S9).

The free energy of unfolding, ΔG°_{u}, for all truncation FhuA derivatives in proteomicelles was surprisingly small, given the expectation that β-barrel membrane proteins exhibit high thermodynamic stability. However, this unexpected outcome is not unique among the examinations of β-barrel proteins. For example, Tamm and colleagues[61] have reported that the free energy of unfolding of OmpA in lipid bilayer is only ~4.5 kcal/mol at pH 7, which is on the same order of magnitude with water-soluble proteins that are closely similar in size. Of course, this small value includes the free energy required for the transfer of all residues into the lipid bilayer (~1 kcal/mol).[62] Moreover, it was recently shown that the 19-strand hVDAC-2 barrel exhibits a relatively low free energy of unfolding in detergent micelles, in the range of 2−5 kcal/mol.[63] The composition of ΔG°_{u} likely encompasses large thermodynamic factors that ultimately offset each other, resulting in a much smaller free energy of unfolding. It is worth mentioning that the interfacial forces at the detergent−protein and lipid−protein interfaces[64] play a pivotal role in modulating these contributions to the free energy of unfolding.

The single-channel electrical recordings involving the transient captures of the N-terminally fused hexahistidine arm by a monoclonal antibody, mAb,[55] demonstrated that this peptide stretch is accessible to the aqueous phase on the periplasmic side of the pore; therefore, it does not undergo excursions from the periplasmic to extracellular sides. Otherwise, these excursions would completely block the pore lumen, closely similar to those current blockades observed with the positively charged Syn B2. The experiments involving the transient long-lived captures of the anti-six-His tag mAb demonstrated the vectorial insertion of truncation FhuA variants with the extracellular loops exposed to the *trans* side and short β-turns exposed to the *cis* side. The hydrophilic tip of the extracellular loops might stochastically partition into transient, very short-lived pores of the lipid bilayer,[65] initiating protein insertion. This finding is in agreement with those of other OM proteins, such as the monomeric mammalian VDAC[66] and trimeric maltoporin (LamB)[67] of *E. coli*, which feature unidirectional insertion into a lipid bilayer. On the other hand, there are other OM proteins, including the monomeric OmpG[68] and trimeric OM protein F (OmpF)[69] of *E. coli*, that insert into a lipid bilayer with no preferred orientation.

We exploited the asymmetric single-channel electrical signature of the hexahistidine arm-containing FhuA in the form of a current−voltage profile and voltage-induced current gating (e.g., uneven current amplitudes and gating fluctuations noted at both transmembrane voltage polarities). These features were coupled with the ability to capture mAb on the *cis* side, but not on the *trans* side. Previously, an engineered disulfide bond between two cysteines on the extracellular loops of OmpG enabled the modulation of the gating fluctuations using a reducing agent added to specific sides of the membrane.[68] Very recently, engineered peripheral cysteines of OmpF were used to produce reversible or nonreversible disulfide reactions with thiol-directed methoxy-poly(ethylene glycol),[69] a reagent previously employed to probe the interior of transmembrane protein pores.[70,71] In both cases, the addition of a sulfhydryl-reactive reagent to a specific side of the chamber revealed the preferred orientation of the protein. Udho et al.[15] found that the osmotic gradient across the lipid bilayer catalyzed the insertion of the FhuA protein into the membrane, but with no preferred orientation. These distinctions between their outcomes and our findings can be explained by the use of different conditions (e.g., with or without an osmotic gradient) as well as different proteins (e.g., FhuA vs heavily truncated hexahistidine arm-containing FhuA protein). Finally, the vectorial insertion of cork-free FhuA variants into a planar lipid bilayer is in excellent accord with its orientation in the OM of *E. coli*, where the large loops face the cytoplasmic compartment of the membrane.

Our experiments with Syn B2 indirectly support the possibility that the 8 nS conductance open state is likely due to a change in the β-barrel conformation. We added the Syn B2 polypeptide to the *trans* side of the chamber and observed an aberrantly increased frequency in the Syn B2-induced current blockades with $H_6[PA]_3$FhuA, as compared with data acquired with TL-FhuA under similar conditions. We rule out the possibility that this effect is due to a direct interaction between Syn B2 and the six-His tag, because of its positioning near the periplasmic side of the pore. Moreover, in the past, we showed that no change in the frequency of binding interactions between a positively charged Syn B2 polypeptide and a protein pore occurs when there is a change in the charge on the opposite side of the polypeptide addition side.[48] Therefore, our experiments with Syn B2 also suggest volumetric changes in the β-barrel conformation.

In summary, the hexahistidine arm-containing truncation FhuA mutant, acquiring an aberrantly high-conductance open state and inserting with a preferred orientation, has prospects for protein engineering in medical molecular biotechnology. Our single-channel electrical recordings with the positively charged Syn B2 polypeptide clearly indicated a poor interaction with TL-FhuA, but a substantially increased frequency of the binding events with $H_6[PA]_3$FhuA, more than likely because of the expanded cross-sectional area of the pore lumen of the latter protein, enabling an increased level of exposure of Syn B2 to more internal acidic residues. Moreover, this study raises awareness among investigators in membrane chemical biology of the potential of a major impact of the fusion of polyhistidine

DOI: 10.1021/acs.biochem.7b00577
Biochemistry 2017, 56, 4895−4905

affinity tags at the terminus side on the pore forming activity of transmembrane proteins. In the future, the preferred orientation will be pivotal for the design of FhuA protein nanopores with controllable gating occlusions that regulate transmembrane transport across lipid vesicles and nanocapsules for drug delivery and biotherapeutics.

■ ASSOCIATED CONTENT

Supporting Information

The Supporting Information is available free of charge on the ACS Publications website at DOI: 10.1021/acs.biochem.7b00577.

Examples of single-channel insertions of individual truncation FhuA derivatives examined in this work, representative single-channel electrical traces and normalized event−amplitude histograms of various truncation FhuA derivatives, representative single-channel electrical traces of various truncation FhuA derivatives at positive and negative voltage biases, representative single-channel electrical traces of $[PA]_3$FhuA, far-ultraviolet CD measurements of various truncation Fhua derivatives in detergent micelles, examination of the thermodynamic stability of various truncation FhuA derivatives using urea-induced unfolding, long-lived captures of the polyhistidine arm of the $H_6[PA]_3$FhuA protein nanopore, which were not noted in the absence of the anti-His mAb, evidence that a hexahistidine peptide arm fused to the C-terminus of FhuA produces unusually high conductance transmembrane protein nanopores, and an illustration of the location of the C- and N-termini, which are in the proximity of the negatively charged cluster of aspartic acids on β-turn T1 (PDF)

■ AUTHOR INFORMATION

Corresponding Author

*Department of Physics, Syracuse University, 201 Physics Building, Syracuse, NY 13244-1130. Phone: 315-443-8078. Fax: 315-443-9103. E-mail: lmovilea@syr.edu.

ORCID

Liviu Movileanu: 0000-0002-2525-3341

Funding

This study was supported by National Institutes of Health Grant GM088403 and National Science Foundation Grant REU DMR-1460784.

Notes

The authors declare no competing financial interest.

■ ACKNOWLEDGMENTS

We thank Stewart Loh for use of a far-ultraviolet CD spectrometer and a Hamilton diluter.

■ REFERENCES

(1) Ayub, M., and Bayley, H. (2016) Engineered transmembrane pores. *Curr. Opin. Chem. Biol. 34*, 117−126.

(2) Slusky, J. S. (2017) Outer membrane protein design. *Curr. Opin. Struct. Biol. 45*, 45−52.

(3) Charan, H., Kinzel, J., Glebe, U., Anand, D., Garakani, T. M., Zhu, L., Bocola, M., Schwaneberg, U., and Boker, A. (2016) Grafting PNIPAAm from beta-barrel shaped transmembrane nanopores. *Biomaterials 107*, 115−123.

(4) Chen, M., Khalid, S., Sansom, M. S., and Bayley, H. (2008) Outer membrane protein G: Engineering a quiet pore for biosensing. *Proc. Natl. Acad. Sci. U. S. A. 105*, 6272−6277.

(5) Mohammad, M. M., Howard, K. R., and Movileanu, L. (2011) Redesign of a plugged beta-barrel membrane protein. *J. Biol. Chem. 286*, 8000−8013.

(6) Grosse, W., Psakis, G., Mertins, B., Reiss, P., Windisch, D., Brademann, F., Burck, J., Ulrich, A., Koert, U., and Essen, L. O. (2014) Structure-based engineering of a minimal porin reveals loop-independent channel closure. *Biochemistry 53*, 4826−4838.

(7) Zhuang, T., and Tamm, L. K. (2014) Control of the Conductance of Engineered Protein Nanopores through Concerted Loop Motions. *Angew. Chem., Int. Ed. 53*, 5897−5902.

(8) Fahie, M., Chisholm, C., and Chen, M. (2015) Resolved single-molecule detection of individual species within a mixture of anti-biotin antibodies using an engineered monomeric nanopore. *ACS Nano 9*, 1089−1098.

(9) Fahie, M. A., Yang, B., Mullis, M., Holden, M. A., and Chen, M. (2015) Selective Detection of Protein Homologues in Serum Using an OmpG Nanopore. *Anal. Chem. 87*, 11143−11149.

(10) Hong, H., Szabo, G., and Tamm, L. K. (2006) Electrostatic couplings in OmpA ion-channel gating suggest a mechanism for pore opening. *Nat. Chem. Biol. 2*, 627−635.

(11) Eren, E., Parkin, J., Adelanwa, A., Cheneke, B. R., Movileanu, L., Khalid, S., and van den Berg, B. (2013) Towards understanding the outer membrane uptake of small molecules by *Pseudomonas aeruginosa*. *J. Biol. Chem. 288*, 12042−12053.

(12) Cheneke, B. R., van den Berg, B., and Movileanu, L. (2015) Quasithermodynamic contributions to the fluctuations of a protein nanopore. *ACS Chem. Biol. 10*, 784−794.

(13) Pothula, K. R., Dhanasekar, N. N., Lamichhane, U., Younas, F., Pletzer, D., Benz, R., Winterhalter, M., and Kleinekathofer, U. (2017) Single Residue Acts as Gate in OccK Channels. *J. Phys. Chem. B 121*, 2614−2621.

(14) Soundararajan, G., Bhamidimarri, S. P., and Winterhalter, M. (2017) Understanding Carbapenem Translocation through OccD3 (OpdP) of Pseudomonas aeruginosa. *ACS Chem. Biol. 12*, 1656−1664.

(15) Udho, E., Jakes, K. S., Buchanan, S. K., James, K. J., Jiang, X., Klebba, P. E., and Finkelstein, A. (2009) Reconstitution of bacterial outer membrane TonB-dependent transporters in planar lipid bilayer membranes. *Proc. Natl. Acad. Sci. U. S. A. 106*, 21990−21995.

(16) Niedzwiecki, D. J., Mohammad, M. M., and Movileanu, L. (2012) Inspection of the Engineered FhuA deltaC/delta4L Protein Nanopore by Polymer Exclusion. *Biophys. J. 103*, 2115−2124.

(17) Udho, E., Jakes, K. S., and Finkelstein, A. (2012) TonB-dependent transporter FhuA in planar lipid bilayers: partial exit of its plug from the barrel. *Biochemistry 51*, 6753−6759.

(18) Zachariae, U., Schneider, R., Briones, R., Gattin, Z., Demers, J. P., Giller, K., Maier, E., Zweckstetter, M., Griesinger, C., Becker, S., Benz, R., de Groot, B. L., and Lange, A. (2012) beta-Barrel mobility underlies closure of the voltage-dependent anion channel. *Structure 20*, 1540−1549.

(19) Teijido, O., Rappaport, S. M., Chamberlin, A., Noskov, S. Y., Aguilella, V. M., Rostovtseva, T. K., and Bezrukov, S. M. (2014) Acidification asymmetrically affects voltage-dependent anion channel implicating the involvement of salt bridges. *J. Biol. Chem. 289*, 23670−23682.

(20) Locher, K. P., Rees, B., Koebnik, R., Mitschler, A., Moulinier, L., Rosenbusch, J. P., and Moras, D. (1998) Transmembrane signaling across the ligand-gated FhuA receptor: crystal structures of free and ferrichrome-bound states reveal allosteric changes. *Cell 95*, 771−778.

(21) Freed, D. M., Lukasik, S. M., Sikora, A., Mokdad, A., and Cafiso, D. S. (2013) Monomeric TonB and the Ton box are required for the formation of a high-affinity transporter-TonB complex. *Biochemistry 52*, 2638−2648.

(22) Hickman, S. J., Cooper, R. E. M., Bellucci, L., Paci, E., and Brockwell, D. J. (2017) Gating of TonB-dependent transporters by substrate-specific forced remodelling. *Nat. Commun. 8*, 14804.

(23) Kim, M., Fanucci, G. E., and Cafiso, D. S. (2007) Substrate-dependent transmembrane signaling in TonB-dependent transporters is not conserved. *Proc. Natl. Acad. Sci. U. S. A. 104*, 11975−11980.
(24) Pawelek, P. D., Croteau, N., Ng-Thow-Hing, C., Khursigara, C. M., Moiseeva, N., Allaire, M., and Coulton, J. W. (2006) Structure of TonB in complex with FhuA, E. coli outer membrane receptor. *Science 312*, 1399−1402.
(25) Ferguson, A. D., Braun, V., Fiedler, H. P., Coulton, J. W., Diederichs, K., and Welte, W. (2000) Crystal structure of the antibiotic albomycin in complex with the outer membrane transporter FhuA. *Protein Sci. 9*, 956−963.
(26) Ferguson, A. D., Kodding, J., Walker, G., Bos, C., Coulton, J. W., Diederichs, K., Braun, V., and Welte, W. (2001) Active transport of an antibiotic rifamycin derivative by the outer-membrane protein FhuA. *Structure 9*, 707−716.
(27) Braun, V. (2009) FhuA (TonA), the career of a protein. *J. Bacteriol. 191*, 3431−3436.
(28) Breyton, C., Flayhan, A., Gabel, F., Lethier, M., Durand, G., Boulanger, P., Chami, M., and Ebel, C. (2013) Assessing the conformational changes of pb5, the receptor-binding protein of phage T5, upon binding to its Escherichia coli receptor FhuA. *J. Biol. Chem. 288*, 30763−30772.
(29) Dezi, M., Di Cicco, A., Bassereau, P., and Levy, D. (2013) Detergent-mediated incorporation of transmembrane proteins in giant unilamellar vesicles with controlled physiological contents. *Proc. Natl. Acad. Sci. U. S. A. 110*, 7276−7281.
(30) Mathavan, I., Zirah, S., Mehmood, S., Choudhury, H. G., Goulard, C., Li, Y., Robinson, C. V., Rebuffat, S., and Beis, K. (2014) Structural basis for hijacking siderophore receptors by antimicrobial lasso peptides. *Nat. Chem. Biol. 10*, 340−342.
(31) Jakes, K. S. (2012) Translocation trumps receptor binding in colicin entry into Escherichia coli. *Biochem. Soc. Trans. 40*, 1443−1448.
(32) Mills, A., Le, H. T., Coulton, J. W., and Duong, F. (2014) FhuA interactions in a detergent-free nanodisc environment. *Biochim. Biophys. Acta, Biomembr. 1838*, 364−371.
(33) Carson, M., Johnson, D. H., McDonald, H., Brouillette, C., and Delucas, L. J. (2007) His-tag impact on structure. *Acta Crystallogr., Sect. D: Biol. Crystallogr. 63*, 295−301.
(34) Li, D. F., Feng, L., Hou, Y. J., and Liu, W. (2013) The expression, purification and crystallization of a ubiquitin-conjugating enzyme E2 from Agrocybe aegerita underscore the impact of His-tag location on recombinant protein properties. *Acta Crystallogr., Sect. F: Struct. Biol. Cryst. Commun. 69*, 153−157.
(35) Thielges, M. C., Chung, J. K., Axup, J. Y., and Fayer, M. D. (2011) Influence of histidine tag attachment on picosecond protein dynamics. *Biochemistry 50*, 5799−5805.
(36) Freydank, A. C., Brandt, W., and Drager, B. (2008) Protein structure modeling indicates hexahistidine-tag interference with enzyme activity. *Proteins: Struct., Funct., Genet. 72*, 173−183.
(37) Dickson, J. M., Lee, W. J., Shepherd, P. R., and Buchanan, C. M. (2013) Enzyme activity effects of N-terminal His-tag attached to catalytic subunit of phosphoinositide-3-kinase. *Biosci. Rep. 33*, 857−863.
(38) Majorek, K. A., Kuhn, M. L., Chruszcz, M., Anderson, W. F., and Minor, W. (2014) Double trouble-Buffer selection and His-tag presence may be responsible for nonreproducibility of biomedical experiments. *Protein Sci. 23*, 1359−1368.
(39) Wolfe, A. J., Mohammad, M. M., Thakur, A. K., and Movileanu, L. (2016) Global redesign of a native beta-barrel scaffold. *Biochim. Biophys. Acta, Biomembr. 1858*, 19−29.
(40) Killmann, H., Benz, R., and Braun, V. (1996) Properties of the FhuA channel in the Escherichia coli outer membrane after deletion of FhuA portions within and outside the predicted gating loop. *J. Bacteriol. 178*, 6913−6920.
(41) Braun, M., Killmann, H., Maier, E., Benz, R., and Braun, V. (2002) Diffusion through channel derivatives of the Escherichia coli FhuA transport protein. *Eur. J. Biochem. 269*, 4948−4959.
(42) Bonhivers, M., Ghazi, A., Boulanger, P., and Letellier, L. (1996) FhuA, a transporter of the Escherichia coli outer membrane, is converted into a channel upon binding of bacteriophage T5. *EMBO J. 15*, 1850−1856.
(43) Mohammad, M. M., Iyer, R., Howard, K. R., McPike, M. P., Borer, P. N., and Movileanu, L. (2012) Engineering a Rigid Protein Tunnel for Biomolecular Detection. *J. Am. Chem. Soc. 134*, 9521−9531.
(44) Mohammad, M. M., Tomita, N., Ohta, M., and Movileanu, L. (2016) The Transmembrane Domain of a Bicomponent ABC Transporter Exhibits Channel-forming Activity. *ACS Chem. Biol. 11*, 2506−2518.
(45) Couoh-Cardel, S., Hsueh, Y. C., Wilkens, S., and Movileanu, L. (2016) Yeast V-ATPase Proteolipid Ring Acts as a Large-conductance Transmembrane Protein Pore. *Sci. Rep. 6*, 24774.
(46) Miles, A. J., and Wallace, B. A. (2016) Circular dichroism spectroscopy of membrane proteins. *Chem. Soc. Rev. 45*, 4859−4872.
(47) Greenfield, N. J. (2007) Using circular dichroism collected as a function of temperature to determine the thermodynamics of protein unfolding and binding interactions. *Nat. Protoc. 1*, 2527−2535.
(48) Wolfe, A. J., Mohammad, M. M., Cheley, S., Bayley, H., and Movileanu, L. (2007) Catalyzing the translocation of polypeptides through attractive interactions. *J. Am. Chem. Soc. 129*, 14034−14041.
(49) Mohammad, M. M., and Movileanu, L. (2008) Excursion of a single polypeptide into a protein pore: simple physics, but complicated biology. *Eur. Biophys. J. 37*, 913−925.
(50) Bikwemu, R., Wolfe, A. J., Xing, X., and Movileanu, L. (2010) Facilitated translocation of polypeptides through a single nanopore. *J. Phys.: Condens. Matter 22*, 454117.
(51) McManus, O. B., and Magleby, K. L. (1988) Kinetic states and modes of single large-conductance calcium-activated potassium channels in cultured rat skeletal-muscle. *J. Physiol. (Oxford, U. K.) 402*, 79−120.
(52) Movileanu, L., Cheley, S., and Bayley, H. (2003) Partitioning of individual flexible polymers into a nanoscopic protein pore. *Biophys. J. 85*, 897−910.
(53) Landry, J. P., Ke, Y., Yu, G. L., and Zhu, X. D. (2015) Measuring affinity constants of 1450 monoclonal antibodies to peptide targets with a microarray-based label-free assay platform. *J. Immunol. Methods 417*, 86−96.
(54) Lindner, P., Bauer, K., Krebber, A., Nieba, L., Kremmer, E., Krebber, C., Honegger, A., Klinger, B., Mocikat, R., and Pluckthun, A. (1997) Specific detection of his-tagged proteins with recombinant anti-His tag scFv-phosphatase or scFv-phage fusions. *BioTechniques 22*, 140−149.
(55) Kaufmann, M., Lindner, P., Honegger, A., Blank, K., Tschopp, M., Capitani, G., Pluckthun, A., and Grutter, M. G. (2002) Crystal structure of the anti-His tag antibody 3D5 single-chain fragment complexed to its antigen. *J. Mol. Biol. 318*, 135−147.
(56) Aguilella-Arzo, M., Aguilella, V. M., and Eisenberg, R. S. (2005) Computing numerically the access resistance of a pore. *Eur. Biophys. J. 34*, 314−322.
(57) Kim, S. C., Kannam, S. K., Harrer, S., Downton, M. T., Moore, S., and Wagner, J. M. (2014) Geometric dependence of the conductance drop in a nanopore due to a particle. *Phys. Rev. E 89*, 042702.
(58) Mapingire, O. S., Henderson, N. S., Duret, G., Thanassi, D. G., and Delcour, A. H. (2009) Modulating effects of the plug, helix, and N- and C-terminal domains on channel properties of the PapC usher. *J. Biol. Chem. 284*, 36324−36333.
(59) Volkan, E., Kalas, V., Pinkner, J. S., Dodson, K. W., Henderson, N. S., Pham, T., Waksman, G., Delcour, A. H., Thanassi, D. G., and Hultgren, S. J. (2013) Molecular basis of usher pore gating in Escherichia coli pilus biogenesis. *Proc. Natl. Acad. Sci. U. S. A. 110*, 20741−20746.
(60) Shuvo, S. R., Ferens, F. G., and Court, D. A. (2016) The N-terminus of VDAC: Structure, mutational analysis, and a potential role in regulating barrel shape. *Biochim. Biophys. Acta, Biomembr. 1858*, 1350−1361.

DOI: 10.1021/acs.biochem.7b00577
Biochemistry 2017, 56, 4895−4905

(61) Tamm, L. K., Hong, H., and Liang, B. (2004) Folding and assembly of beta-barrel membrane proteins. *Biochim. Biophys. Acta, Biomembr. 1666*, 250−263.
(62) White, S. H., and Wimley, W. C. (1999) Membrane protein folding and stability: physical principles. *Annu. Rev. Biophys. Biomol. Struct. 28*, 319−365.
(63) Maurya, S. R., and Mahalakshmi, R. (2013) Modulation of human mitochondrial voltage-dependent anion channel 2 (hVDAC-2) structural stability by cysteine-assisted barrel-lipid interactions. *J. Biol. Chem. 288*, 25584−25592.
(64) Wolfe, A. J., Hsueh, Y. C., Blanden, A. R., Mohammad, M. M., Pham, B., Thakur, A. K., Loh, S. N., Chen, M., and Movileanu, L. (2017) Interrogating Detergent Desolvation of Nanopore-Forming Proteins by Fluorescence Polarization Spectroscopy. *Anal. Chem. 89*, 8013−8020.
(65) Movileanu, L., Popescu, D., Ion, S., and Popescu, A. I. (2006) Transbilayer pores induced by thickness fluctuations. *Bull. Math. Biol. 68*, 1231−1255.
(66) Sheldon, K. L., Maldonado, E. N., Lemasters, J. J., Rostovtseva, T. K., and Bezrukov, S. M. (2011) Phosphorylation of voltage-dependent anion channel by serine/threonine kinases governs its interaction with tubulin. *PLoS One 6*, e25539.
(67) Gurnev, P. A., Oppenheim, A. B., Winterhalter, M., and Bezrukov, S. M. (2006) Docking of a single phage lambda to its membrane receptor maltoporin as a time-resolved event. *J. Mol. Biol. 359*, 1447−1455.
(68) Chen, M., Li, Q. H., and Bayley, H. (2008) Orientation of the monomeric porin OmpG in planar lipid bilayers. *ChemBioChem 9*, 3029−3036.
(69) Ionescu, S. A., Lee, S., Housden, N. G., Kaminska, R., Kleanthous, C., and Bayley, H. (2017) Orientation of the OmpF Porin in Planar Lipid Bilayers. *ChemBioChem 18*, 554−562.
(70) Movileanu, L., and Bayley, H. (2001) Partitioning of a polymer into a nanoscopic protein pore obeys a simple scaling law. *Proc. Natl. Acad. Sci. U. S. A. 98*, 10137−10141.
(71) Movileanu, L., Cheley, S., Howorka, S., Braha, O., and Bayley, H. (2001) Location of a constriction in the lumen of a transmembrane pore by targeted covalent attachment of polymer molecules. *J. Gen. Physiol. 117*, 239−251.

DOI: 10.1021/acs.biochem.7b00577
Biochemistry 2017, 56, 4895−4905